https://doi.org/10.18321/ectj1496

Preparation of C_{60} Fullerene Nanowhisker–CuS Nanoparticle Composites and Photocatalyst for Rhodamine B Degradation under Blue Light Emitting Diode Irradiation

S.W. Ko and H. Chung*

Department of Convergence Science, Graduate School, Sahmyook University, 815, Seoul 139-742, South Korea

Article info

Received:
19 January 2023

Received in revised form:
15 March 2023

Accepted:
24 April 2023

Keywords:
Liquid-liquid interfacial precipitation;
C_{60} FNW-CuS nanoparticle composites;
Photocatalytic degradation;
Rhodamine B;
Blue LED irradiation.

Abstract

The liquid-liquid interfacial precipitation (LLIP) approach was used to synthesize the C_{60} fullerene nanowhisker (FNW)–CuS nanoparticle composites utilizing a CuS nanoparticle solution, C_{60}-saturated toluene, and isopropyl alcohol (IPA). Powder X-ray diffraction (XRD), Raman spectroscopy, scanning electron microscopy (SEM), and transmission electron microscopy (TEM) were used to characterize the product of C_{60} FNW–CuS nanoparticle composites. These were also utilized to photocatalytic degradation of rhodamine B (RhB) under blue light emitting diode (LED) irradiation at 450 nm. Also, UV–vis spectroscopy was used to confirm the photocatalytic degradation activity of RhB over the C_{60} FNW–CuS nanoparticle composites. The percentage of photocatalytic degradation of RhB was shown to be 95.148%. The kinetics study for photocatalytic degradation of RhB using C_{60} FNW–CuS nanoparticle composites followed a pseudo-first-order reaction rate law. C_{60} FNW–CuS nanoparticle composites as photocatalyst have a rate constant of 4.82×10^{-2} min^{-1} at 25 °C.

1. Introduction

Environmental scientists are very interested in the use of photocatalysis for problems like the treatment of dyes, organic contaminants, and the cleaning of contaminated water [1]. The environment and human health are seriously at risk due to rising water contamination from various sources, including industrial effluents, chemical spills, and agricultural runoff [2]. In particular, wastewater released from industries such as textiles, printing, leather, and cosmetics contains a considerable amount of various types of dyes, which are known to cause the most serious pollution among various water pollutants [3]. Due to their enormous potential as heterogeneous photocatalysts, semiconductor nanoparticles have attracted a lot of interest in the application field of environmental remediation technologies during the past few decades [4, 5]. The phenomenon of photocatalytic activity for splitting water into oxygen and hydrogen was discovered with titanium oxide under ultraviolet irradiation [6]. The application of TiO_2-based nanocomposites is the purification of water by photocatalytic degradation of organic dyes under ultraviolet irradiation [7, 8]. Among semiconductor nanoparticles, owing to their distinctive physical and chemical characteristics, copper sulfide (CuS) nanoparticles have been extensively used among metal sulfide nanoparticles. One of the p-type semiconductors, CuS nanoparticles exist in different crystalline phase with various optical properties [9]. Copper sulfide nanoparticles have been synthesized from various methods such as sonochemical [10], solvothermal [11], microwave [12], hydrothermal [13], and colloidal [14]. The band gap energy of copper sulfide ranges from 1.2~5.08 eV [15, 16]. The energy band gap is affected by the crystalline phase, particle size, and synthetic methods.

*Corresponding author.
E-mail address: larus@nate.com

As photocatalyst, the greenish-black solid, CuS nanoparticles have been utilized to degrade organic dyes like MB, MO, and RhB [2, 17]. Meng et al. discovered an efficient catalytic property for the degradation of RhB using a hierarchical CuS hollow nanosphere [2]. In addition, CuS nanoparticles have shown outstanding photodegradation and quick dye adsorption capabilities for organic dyes in aqueous solution [2]. Recently, interest in C_{60} fullerene nanowhiskers has increased due to their distinct chemical and physical characteristics, as well as potential uses in materials like catalysis and photocatalysis [18–25]. The C_{60} fullerene nanowhiskers of the needle-like crystals were prepared by the liquid-liquid interfacial precipitation (LLIP) method using a C_{60}-saturated toluene and isopropyl alcohol [26]. We applied the liquid-liquid interfacial precipitation to the system of ethanol solution of CuS, saturated toluene solution of C_{60}, and isopropyl alcohol and have discovered that needle-like crystalline precipitates of hybrid C_{60} FNW–CuS nanoparticle composites are formed in the solution [26]. C_{60} fullerene nanowhiskers may act as an n-type semiconducting materials and have been used in various applications, including catalysts, photocatalysts, chemical sensors, solar cells, and field-effect transistors [27]. The RhB dye was selected as a model contaminant because it is usually present in wastewater from several industries, including the textile and food industries [28]. That's the reason why we chose to use RhB dye as a model contaminant for the photodegradation experiments.

In this study, we evaluated the photocatalytic activity and the kinetics study for the degradation of RhB using hybrid C_{60} FNW–CuS nanoparticle composites under blue LED irradiation at 450 nm by employing UV–vis spectrophotometry.

2. Experimental

2.1. Materials and instruments

Copper (II) nitrate trihydrate ($Cu(NO_3)_2 \cdot 3H_2O$), sodium sulfide nonahydrate ($Na_2S \cdot 9H_2O$), rhodamine B ($C_{28}H_{31}ClN_2O_3$), and toluene (C_7H_8) were obtained from Sigma-Aldrich (USA). Ethylene glycol ($C_2H_6O_2$) and ethanol (C_2H_5OH) were supplied by Daejung Chemicals (Korea). C_{60} fullerene was bought from Tokyo Chemical Industry Co., Ltd (Japan). Powder X-ray diffraction (Bruker, D8 Advance, Germany) was used to analyze the sample's crystal structure at 40 kV and 40 mA. Raman spectroscopy (B&W Tek i-Raman plus instrument, BWS465-532S, USA) was carried out to analyze the lattice vibrations of the sample. Scanning electron microscopy (SEM; JSM-6510, JEOL Ltd., Japan) was conducted at an accelerating voltage of 15 kV, and a magnification of the surface morphology of the sample 8500 X. Transmission electron microscopy (TEM; AP Tech, G2 F30 S-Twin, Tecnai, USA) measurement was conducted at an acceleration voltage of 100 kV ~300 kV to determine the particle size and shape of the samples. UV–vis spectrophotometry (Lambda 365 UV/Vis, Perkin Elmer, USA) was used to evaluate the photocatalytic activity and kinetics study for degradation of RhB under blue LED irradiation at 450 nm. LED lamp (10W, 450 nm, LED T5 Jinsung Electronic., Ltd, China) was used for light irradiation.

2.2. Synthesis of CuS nanoparticles

Copper (II) nitrate trihydrate ($Cu(NO_3)_2 \cdot 3H_2O$) (0.48 g) as a copper precursor and sodium sulfide nonahydrate ($Na_2S \cdot 9H_2O$) (0.48 g) as a sulfur precursor were dissolved into ethylene glycol ($C_2H_6O_2$) and then stirred the solution at 20 °C for 12 h. After the reaction, the precipitate was collected by centrifugation and dried at 60 °C for 2 h to obtain the solid state CuS nanoparticles.

2.3. Synthesis of C_{60} FNW–CuS nanoparticle composites

The CuS nanoparticles solution was prepared by dissolving 30 mg of powdered CuS nanoparticles in 30 mL of ethanol (C_2H_5OH) solution. The C_{60} FNW–CuS nanoparticle composites were synthesized by liquid-liquid interfacial precipitation (LLIP) method using 5 mL of CuS nanoparticles solution, 10 mL of C_{60}-saturated toluene, and 75 mL of isopropyl alcohol.

2.4. Photocatalytic activity and kinetics study for degradation of RhB using C_{60} FNW–CuS nanoparticle composites

The photocatalytic degradation of RhB was conducted by adding 10 mL of 0.01 mM RhB into a 10 mL of glass vial containing 8 mg of C_{60} FNW–CuS nanoparticle composites as photocatalyst. The solution was kept in a dark condition for

60 min to achieve an adsorption-desorption equilibrium between the photocatalyst and RhB. The photocatalytic activity and kinetic study for degradation of RhB over the C_{60} FNW–CuS nanoparticle composites under blue LED irradiation at 450 nm for 10 min interval were monitored using UV–vis spectroscopy.

3. Results and discussion

3.1. Characterization of C_{60} FNW–CuS nanoparticle composites

The crystal structure and crystallite size of the C_{60} FNW–CuS nanoparticle composites were confirmed by powder X-ray diffraction. As shown in Fig. 1, the peaks at 10.85°, 17.74°, 20.68°, 28.12°, 30.86°, and 32.77° correspond to the (110), (222), (311), (420), (422), and (333) planes due to the C_{60} fullerene nanowhiskers, respectively. In addition, the peaks at 27.69°, 29.42°, 32.63°, 48.10°, and 59.30° correspond to (101), (102), (006), (110) and (116) planes of the CuS nanoparticles in Fig. 1, respectively (JCPDS No. 06-0464) [24].

Therefore, XRD data show that C_{60} FNW–CuS nanoparticle composites were successfully synthesized. In addition, the average crystallite size of CuS nanoparticles was estimated by Scherrer's Eq. (1):

$$D = \frac{K\lambda}{\beta \cos\theta} \quad (1)$$

where D is the crystallite size, λ is the wavelength of X-ray diffraction with CuKα radiation (λ = 0.154 nm), K is a shape factor (taken 0.9), 2θ is the angle between the incident and the scattered X-rays, and β is the full width at half maximum intensity (FWHM). The average crystallite size of the CuS nanoparticles was determined to be 12.72 nm, in Table 1.

Table 1
The Crystallite size of the CuS nanoparticles evaluated using the Scherrer equation in the C_{60} FNW–CuS nanoparticle composites.

Compound	Plane (hkl)	2θ (degree)	FWHM (degree)	Crystallite size (nm)
CuS NPTs	101	27.69	0.62	13.79
	102	29.42	0.60	14.30
	006	32.63	1.16	7.46
	110	48.10	0.67	13.57
	116	59.30	0.66	14.47
Average				12.72

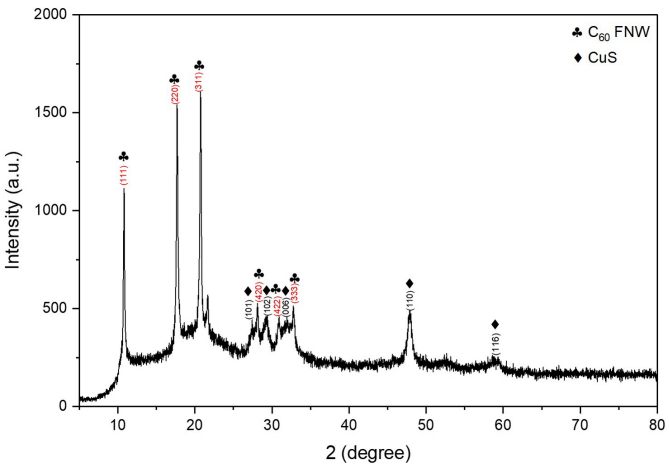

Fig. 1. XRD pattern of C_{60} FNW–CuS nanoparticle composites.

Figure 2 shows the Raman spectrum of the C_{60} FNW–CuS nanoparticle composites. Raman shift of the C_{60} FNW–CuS composites appeared Hg(1) at 269 cm^{-1}, Ag(1) at 490 cm^{-1}, Ag(2) at 1458 cm^{-1} due to the C_{60} fullerene nanowhiskers and at 461 cm^{-1} due to the CuS nanoparticles [29].

Figure 3 shows an SEM image of the C_{60} FNW–CuS nanoparticle composites. The SEM image shows that the C_{60} fullerene nanowhisker have a rod like structure. The agglomerated CuS nanoparticles located on the C_{60} fullerene nanowhiskers.

Figure 4 shows TEM image of the C_{60} FNW–CuS nanoparticle composites. The TEM image shows that CuS nanoparticles are agglomerated and adhere to C_{60} fullerene nanowhiskers. The width of the hybrid nanocomposites is about 550 nm, and the size of CuS nanoparticles is 10~138 nm.

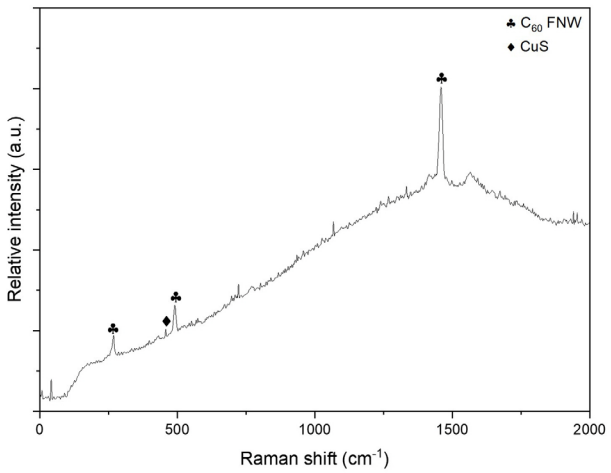

Fig. 2. Raman spectrum of C_{60} FNW–CuS nanoparticle composites.

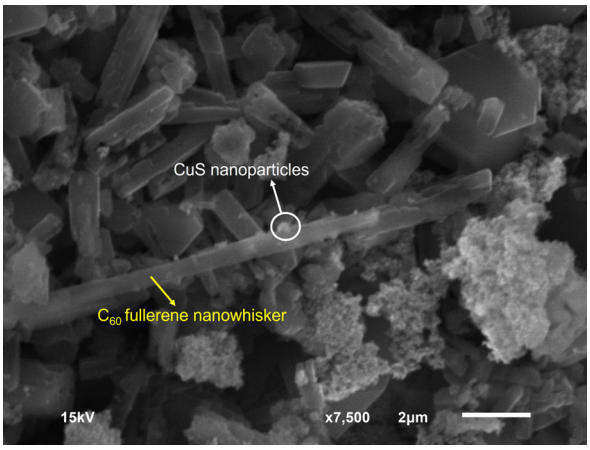

Fig. 3. SEM image of C_{60} FNW–CuS nanoparticle composites.

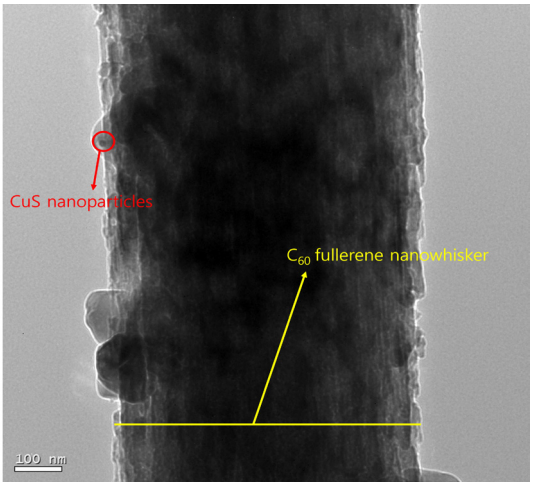

Fig. 4. TEM image of C_{60} FNW–CuS nanoparticle composites.

The EDX spectrum for the elemental composition of the synthesized of C_{60} fullerene nanowhisker–CuS nanoparticle composites is shown in Fig. 5.

According to the EDX spectrum, the C_{60} fullerene nanowhisker–CuS nanoparticle composites contained a copper atom of 7.37%, a sulfur atom of 4.34%, and a carbon atom of 88.29%.

3.2. Photocatalytic activity and kinetics study for the degradation of RhB using C_{60} FNW–CuS nanoparticle composites as photocatalyst

Figure 5 shows UV-vis spectrum for photocatalytic degradation of RhB in the presence of C_{60} FNW–CuS nanoparticle composites as photocatalyst. The percentage for degradation of RhB using C_{60} FNW–CuS nanoparticle composites appeared in Table 2.

The percentage of degradation of RhB was calculated using the following equation [30]; Eq. (2)

$$RhB = (C_0\text{-}C)/C_0 \text{ X } 100\% \quad (2)$$

where C_0 is the initial concentration of RhB after adsorption for 60 min and C is the concentration of RhB at time t. Both C_0 and C values were obtained from the maximum absorption at 554 nm in the UV–vis absorption spectrum. C_{60} FNW–CuS nanoparticle composites were used, they showed 95.148% of RhB decomposition under blue LED irradiation at 450 nm.

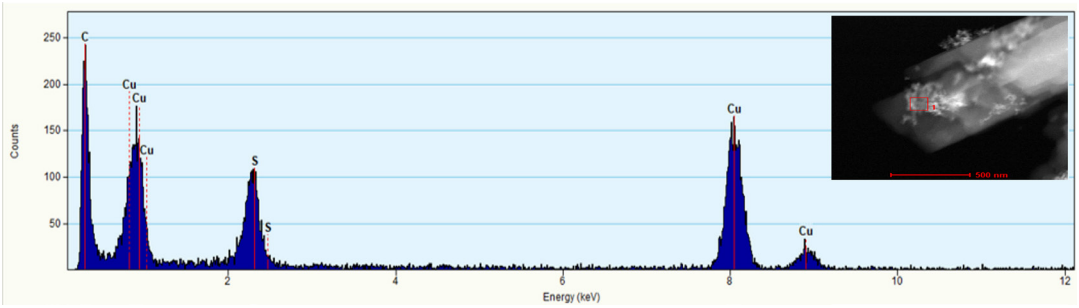

Fig. 5. EDX spectrum for elemental analysis of C_{60} FNW–CuS nanoparticle composites.

Table 2
Percentage of photocatalytic degradation of RhB using on C_{60} FNW–CuS nanoparticle composites as catalyst after adsorption for 60 min.

Time (min)	60	70	80	90	100	110	120
Concentration of RhB (C)	0.4143	0.2354	0.1477	0.0996	0.0600	0.0412	0.0201
Percentage of photocatalytic degradation of RhB (%)	0.000	43.1813	64.3495	75.9594	85.5177	90.0555	95.1484

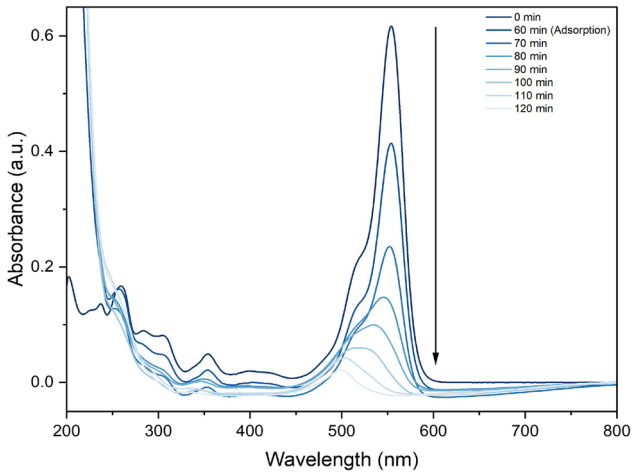

Fig. 6. UV-vis spectra of catalytic degradation of RhB under blue LED irradiation at 450 nm using on C_{60} FNW–CuS nanoparticle composites.

Figure 6 shows the results of the kinetics study for the photocatalytic degradation of RhB with C_{60} FNW–CuS nanoparticle composites under blue LED irradiation at 450 nm. The equation for the first order reaction kinetics is as follows [31]; Eq. (3)

$$\ln(C/C_0) = -kt \quad (3)$$

in which k is the rate constant, C_0 is the initial concentration and C is the concentration at time t.

The linear behavior of the slope indicates that the photocatalytic degradation of RhB over the hybrid nanocomposites followed pseudo-first order kinetics in Fig. 7. The rate constant (k) of C_{60} FNW–CuS nanoparticle composites is 4.817×10^{-2} min^{-1} at 25 °C. If the value of R^2 (coefficient of determination) is close to 1, the kinetics obey a first-order reaction. Therefore, because the R^2 value was 0.994, the kinetics followed a pseudo-first-order reaction.

3.3. Mechanism of photocatalytic degradation of RhB by C_{60} FNW–CuS nanoparticle composites

The mechanism of photocatalytic degradation for RhB based on C_{60} FNW–CuS nanoparticle composites in Fig. 8 can be summarized by the following Eqs. (4-7):

$$C_{60}FNW/CuS \xrightarrow{h\nu(450\,nm)} C_{60}FNW(e^-)/CuS(h^+) \quad (4)$$

$$CuS\,(h^+) + OH^- \rightarrow CuS + \cdot OH \quad (5)$$

$$C_{60}FNW\,(e^-) + O_2 \rightarrow C_{60}FNW + \cdot O_2^- \quad (6)$$

$$RhB + (\cdot OH, \cdot O_2^-) \rightarrow CO_2 + H_2O + \text{Inorganic Salts} \quad (7)$$

When the photon energy is greater than the band gap energy of a copper sulfide CuS nanoparticle irradiating its surface, the electrons in the valence band are excited to the conduction band. This resulted in the continuous generation of holes (h^+) in the valence band and electrons (e^-) in the conduction band. The CuS nanoparticles were photogenerated electrons, and their electrons tend to transfer to the LUMO of C_{60} fullerene nanowhisker (Eq. (4)), leading to efficient electron-hole separation. These separated electrons and holes are trapped by some surface adsorbates to generate reactive radical species. The holes left in the CuS valence band can react with adsorbed water(or hydroxyl) to form hydroxy radicals (·OH) (Eq. (5)) and electrons stored in C_{60} fullerene nanowhisker are trapped by O_2 to form a reactive superoxide radical ion ($\cdot O_2^-$) (Eq. (6)). Both radical groups ($\cdot O_2^-$ and ·OH) are reactive toward RhB dye degradation and finally form CO_2, H_2O, and inorganic salts (Eq. (7)). The roles of the CuS nanoparticles were photogenerated electrons in the photocatalyst, and the C_{60} fullerene nanowhisker were trapped electrons, thus preventing their recombination with photogenerated holes [32]. It is well known that C_{60} fullerene nanowhisker is an excellent electron acceptor, which could trapped the conduction band electron of CuS [33]. This is the dominant mechanism resulting in the enhanced photocatalytic degradation performance of the C_{60} fullerene nanowhisker–CuS nanoparticle composites compared to bare CuS.

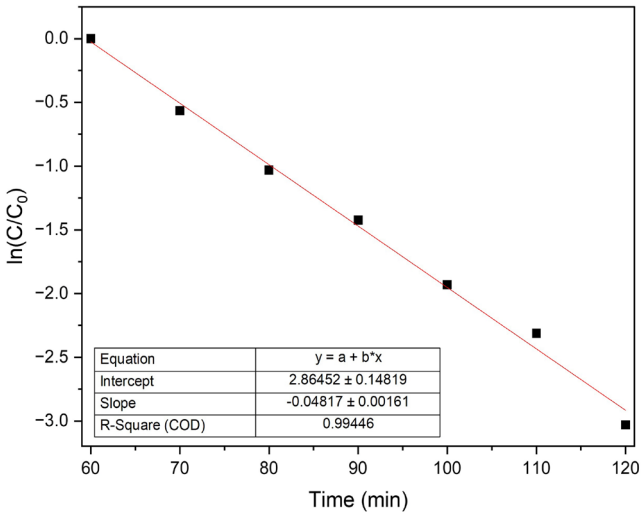

Fig. 7. Kinetics study for degradation of RhB using on C_{60} FNW–CuS nanoparticle composites as photocatalyst under blue LED irradiation at 450 nm.

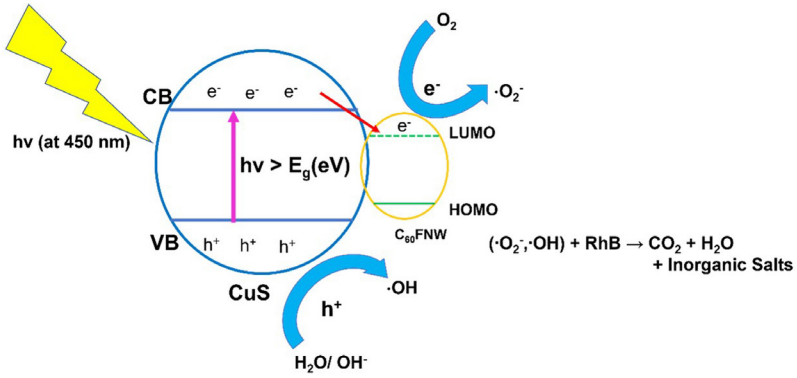

Fig. 8. Mechanism of photocatalytic degradation of RhB by C_{60} FNW–CuS nanoparticle composites.

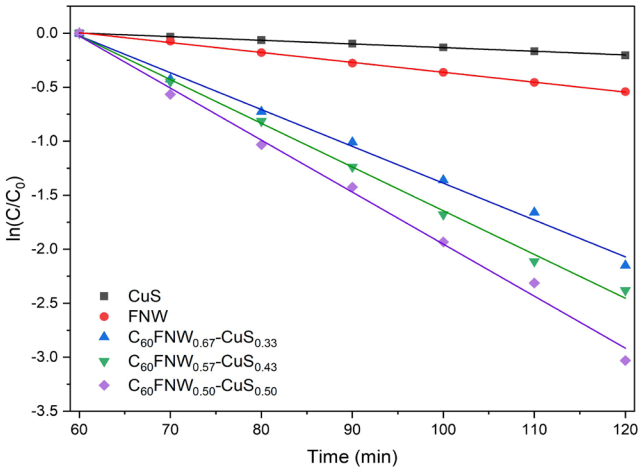

Fig. 9. Effect on the photocatalytic degradation of RhB by C_{60} FNW–CuS nanoparticle composites depend on the quantity ratio of C_{60} fullerene nanowhisker and CuS nanoparticle (Experimental conditions: initial dye concentration 0.01 mM; wavelength of LED irradiation: 450 nm; photocatalyst concentration: 0.8 g/L).

3.4. Effect on the photocatalytic degradation of RhB by the C_{60} FNW–CuS nanoparticle composites depend on the quantity ratio of C_{60} fullerene nanowhisker and CuS nanoparticle

The photocatalytic degradation performance of RhB dye was investigated under various photocatalyst conditions in Fig. 9.

Also, the efficiency and reaction rate constant for photocatalytic degradation of RhB using various photocatalysts are presented in Table 3.

The rate for photocatalytic degradation of RhB was fastest, the efficiency was highest at 95.148%, and the reaction rate constant was 4.82×10^{-2} min^{-1} when the quantity ratio of C_{60} fullerene nanowhisker and CuS nanoparticle was 0.5 and 0.5, respectively.

Table 3
Efficiency and reaction rate constants for the degradation of RhB using photocatalysts.

Compound	Reaction rate constant k (min^{-1})	Photocatalytic degradation efficiency (%)
CuS	0.0034	18.44
FNW	0.0092	41.77
$C_{60}FNW_{0.67}$-$CuS_{0.33}$	0.0341	88.35
$C_{60}FNW_{0.57}$-$CuS_{0.43}$	0.0409	90.73
$C_{60}FNW_{0.50}$-$CuS_{0.50}$	0.0482	95.148

4. Conclusion

The C_{60} fullerene nanowhisker–CuS nanoparticle composites were prepared by the LLIP method using CuS nanoparticles solution, a saturated solution of C_{60} fullerene in toluene, and isopropyl alcohol. The prepared hybrid nanocomposites were characterized using XRD, Raman spectroscopy, SEM, and TEM. Photocatalytic degradation of RhB was performed using C_{60} FNW–CuS nanoparticle composites under blue LED irradiation at 450 nm.

The rate for photocatalytic degradation of RhB was the fastest, the efficiency is highest as 95.148%, and the reaction rate constant was 4.82×10^{-2} min^{-1} at 25 °C when the quantity ratio of C_{60} fullerene nanowhisker and CuS nanoparticle was 0.5 and 0.5, respectively.

The kinetics of the photocatalytic degradation of RhB with photocatalyst followed the pseudo-first order reaction rate law. Future research will further measure the recycling RhB degradation test to investigate the photocatalytic stability of C_{60} fullerene nanowhisker–CuS nanoparticle composites under blue light emitting diode irradiation.

Acknowledgements

This study was supported by research funding from Sahmyook University in Korea.

References

[1]. M. Saranya, R. Ramachandran, E.J.J. Samuel, et al., *Powder Technol.* 279 (2015) 209–220. DOI: 10.1016/j.powtec.2015.03.041

[2]. M. Pal, N.R. Mathews, E. Sanchez-Mora, et al., *J. Nanoparticle Res.* 17 (2015). DOI: 10.1007/s11051-015-3103-5

[3]. G.M. Neelgund, A. Oki, *Mater. Res. Bull.* 129 (2020) 110911. DOI: 10.1016/j.materresbull.2020.110911

[4]. M.R. Hoffmann, S.T. Martin, W. Choi, D.W. Bahnemann, *Chem. Rev.* 95 (1995) 69–96. DOI: 10.1021/cr00033a004

[5]. X. Meng, G. Tian, Y. Chen, et al., *Cryst. Eng. Comm.* 15 (2013) 5144–5149. DOI: 10.1039/C3CE40195B

[6]. A. Fujishima, K. Honda, *Nature* 238 (1972) 37–38. DOI: 10.1038/238037a0

[7]. A. Fujishima, T.N. Rao, D.A. Tryk, *J. Photochem. Photobiol. C.* 1 (2000) 1–21. DOI: 10.1016/S1389-5567(00)00002-2

[8]. D. Chenchik, J. Jandosov, *Eurasian Chem.-Technol. J.* 19 (2017) 191–195. DOI: 10.18321/ectj651

[9]. S. Yadav, P.K. Bajpai, *Nano-Struct. Nano-Objects* 10 (2017) 151–158. DOI: 10.1016/j.nanoso.2017.03.009

[10]. A. Singh, R. Manivannan, S.N. Victoria, *Arab. J. Chem.* 12 (2019) 2439–2447. DOI: 10.1016/j.arabjc.2015.03.013

[11]. M. Jain, D.G. Babar, S.S. Garje, *Appl. Nanosci.* 9 (2019) 353–367. DOI: 10.1007/s13204-018-0915-5

[12]. D. Rohilla, N. Kaur, A. Shanavas, S. Chaudhary, *Chemosphere* 277 (2021) 130202. DOI: 10.1016/j.chemosphere.2021.130202

[13]. S.S.T. Selvi, J.M. Linet, S. Sagadevan, *J. Exp. Nanosci.* 13 (2018) 130–143. DOI: 10.1080/17458080.2018.1445306

[14]. Y. Zhai, M. Shim, *Chem. Mater.* 29 (2017) 2390–2397. DOI: 10.1021/acs.chemmater.7b00461

[15]. L. Isac, I. Popovici, A. Enesca, A. Duta, *Energy Procedia* 2 (2010) 71–78. DOI: 10.1016/j.egypro.2010.07.013

[16]. S.I. Raj, A. Jaiswal, I. Uddin, *RSC Adv.* 10 (2020) 14050–14059. DOI: 10.1039/C9RA09306K

[17]. M. Baláž, E. Dutková, Z. Bujňáková, et al., *J. Alloys Compd.* 746 (2018) 576–582. DOI: 10.1016/j.jallcom.2018.02.283

[18]. T. Wakahara, K. Miyazawa, Y. Nemoto, O. Ito, *Carbon* 49 (2011) 4644–4649. DOI: 10.1016/j.carbon.2011.06.041

[19]. K. Miyazawa, K. Hamamoto, *J. Mater. Sci. Res.* 17 (2002) 2205–2208. DOI: 10.1557/JMR.2002.0325

[20]. K. Miyazawa, K. Hamamoto, S. Nagata, T. Suga, *J. Mater. Sci. Res.* 18 (2003) 1096–1103. DOI: 10.1557/JMR.2003.0151

[21]. T. Wakahara, M. Sathish, K. Miyazawa, T. Sasaki, *Nano* 3 (2008) 351–354. DOI: 10.1142/S1793292008001180

[22]. K. Miyazawa, *J. Nanosci. Nanotechnol.* 9 (2009) 41–50. DOI: 10.1166/jnn.2009.J013

[23]. J.W. Ko, W.B. Ko, *Mater. Trans.* 57 (2016) 2122–2126. DOI: 10.2320/matertrans.M2016214

[24]. J.W. Ko, K. Miyazawa, Y. Tanaka, W.B. Ko, *Fuller. Nanotub. Carbon Nanostructures* 28 (2020) 794–798. DOI: 10.1080/1536383X.2020.1762078

[25]. J.W. Ko, W.B. Ko, *Fuller. Nanotub. Carbon Nanostructures* 25 (2017) 710–715. DOI: 10.1080/1536383X.2017.1377698

[26]. K. Miyazawa, Y. Kuwasaki, A. Obayashi, M. Kuwabara, *J. Mater. Sci. Res.* 17 (2002) 83–88. DOI: 10.1557/JMR.2002.0014

[27]. F. Sica, S. Adinolfi, L. Vitagliano, et al., *J. Cryst. Growth* 168 (1996) 192–197. DOI: 10.1016/0022-0248(96)00354-5

[28]. B. Xing, C. Shi, C. Zhang, et al., *J. Nanomater.* 2016 (2016) 8393648. DOI: 10.1155/2016/8393648

[29]. Y. Wang, F. Jiang, J. Chen, et al., *J. Nanomater.* 10 (2020) 178. DOI: 10.3390/nano10010178

[30]. J.W. Ko, W.B. Ko, *Fuller. Nanotub. Carbon Nanostructures* 27 (2019) 895–898. DOI: 10.1080/1536383X.2019.1657416

[31]. J.W. Ko, W.B. Ko, *Fuller. Nanotub. Carbon Nanostructures* 30 (2022) 693–698. DOI: 10.1080/1536383X.2021.2008368

[32]. J. Yu, T. Ma, G. Liu, B. Cheng, *Dalton Trans.* 40 (2011) 6635–6644. DOI: 10.1039/C1DT10274E

[33]. K. Miyazawa, M. Tachibana, S. Nakamura, T. Kizuka, Y. Ochiai, Fullerene Nanowhiskers. Pan Stanford, Singapore, 2019, p. 190. DOI: 10.1201/9781351042147